Spline-based helicopter movement filter for sea ice surface topography estimation from airborne laser range finder

Jean NEGREL[a,b], Dmitry V. DIVINE[a], Sebastian GERLAND[a]

[a] *Norwegian Polar Institute, Fram Centre, Postboks 6606 Stakkevollan, Tromsø, NO-9296, Norway*
[b] *Now at: NORCE Norwegian Research Centre, Postboks 22 Nygaardstangen, Bergen, NO-5838, Norway*

Abstract

The surface topography of sea ice is important for several crucial climate processes, such as atmosphere-ice interaction, sea ice drift, snow redistribution and habitat conditions. A method, derived from the widely used three-steps Hibler filter, is suggested to gain quantitative surface topography information from airborne surveys over sea ice, when laser range finder are used. The method was tested and validated for several segments of a helicopter flight over Arctic sea ice. It was compared to a DTM generated from stereo-photogrammetry data collected simultaneously and independently from the laser data. The estimated ice surface profiles matched the reference DTM with an average absolute bias of 0.12 m.

Keywords: Sea ice, surface topography, laser range finder, airborne

Email address: `jean.negrel@norceresearch.no` (Jean NEGREL)

1. Introduction

Arctic sea ice processes play an important role in climate dynamics, local environment, shipping and tourism [1, 2]. In particular, the sea ice surface topography affects the atmosphere-ice-ocean interaction [3, 4], ice drift, snow redistribution [5, 6] and energy transfer, through the influence of summer melt [7, 8].

The use of laser range finders (LRF) or scanners has now well proven its efficiency in characterising the morphology of the sea ice surfaces [9, 10, 11].

However, in some applications like for example helicopter-borne electromagnetic sounding of sea ice (HEM) [12], LRF is used in the first place as an auxiliary setup only, not integrated with the GNSS and/or inertial navigation system unit. Then, the vertical motion of the aircraft blends in the recorded signal. With the amplitude of the aircraft motion being one to two order of magnitude higher than variation of the ice surface topography, the filtering procedure represents a crucial step in the processing of such data.

The three steps filter proposed by [13] has been used widely to estimate and remove the aircraft motion from the recorded signal. Although quite simple to implement and very efficient on short flight segments (<1 km long), this procedure show its limits when processing longer flights segments, in particular in the case of helicopter-borne surveys, because they potentially can exhibit higher variability in altitude over shorter distances than planes. The discontinuous nature of the procedure can also introduce distortions in the resulting signal.

Inspired by the procedure developed by [13], we here propose a spline-based helicopter motion filter to estimate sea ice surface topography from

LRF. We applied and tested the method on a dataset collected over Arctic sea ice and compared it to a digital terrain model (DTM), created from independent, simultaneously collected data.

2. Helicopter movement filter

The principle of the Hibler filter [13] for deriving ice surface topography along flight lines relies on the assumption that the LRF signals from an airborne platform comprise a relatively easy to disentangle superposition of returns at a higher frequency, originating from the ice surface signal, and lower frequency, originating from the aircraft motion. This assumption may fit the reality quite well in the case of an airplane, with a fairly constant flying speed. However, a helicopter can exhibit a much more complex motion profile with the potential of more abrupt movements (although pilots usually avoid this). In particular, helicopters have the possibility of changing altitude at very low horizontal speed, resulting in effects of vertical helicopter motion to leak into the high frequencies part of the altimeter series.

We here tested an empirical approach for the filtering of the helicopter movement, based on the combination of the frequency analysis of the signal and the estimation of the envelope of the signal. The proposed approach is based on the assumption of the local maxima in the recorded raw laser range profile, primarily associated with cracks and leads, which are common features in the sea ice (Fig.1). These features can serve as reference points creating a baseline to estimate the vertical motion of the helicopter, relative to the sea level. It must be noted that depressions in the ice pack would also appear as local minima in surface topography without necessary corresponding to the sea level. A careful inspection of the recorded signal along with flight notes can help to connect visually observed cracks and leads to the respective altimeter data.

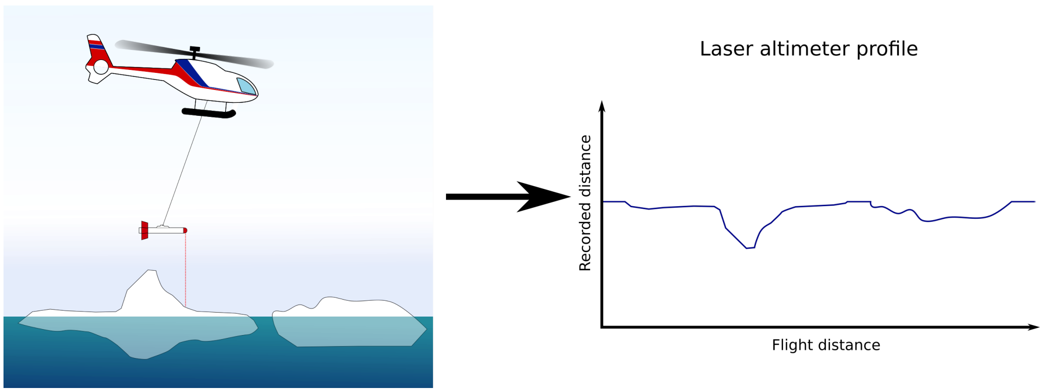

Figure 1: Schematic representation of a flight profile as recorded from the LRF of the HEM under ideal conditions (constant elevation relative to water surface). Lower distances for an idealistic level flight case correspond to ridges while higher distances correspond to cracks and open water.

Hence, we aim to recover the true motion of a helicopter relative to the local ocean surface using the estimation of a curve passing the largest recorded distance along the transect. Given that pilots usually steer helicopters in a way that they do not stop abruptly in horizontal flying direction, one can expect smooth transitions in the vertical motion of the aircraft. Hence, we can assume the helicopter motion to be continuous and fully differentiable along a flight track. So, the elevation data for the transitions can be approximated by a polynomial function and estimated through a spline interpolation between the selected reference points.

For calculating the vertical motion profile along the flight distance, a two-step procedure is proposed, 1) filtering the raw LRF profile to isolate in

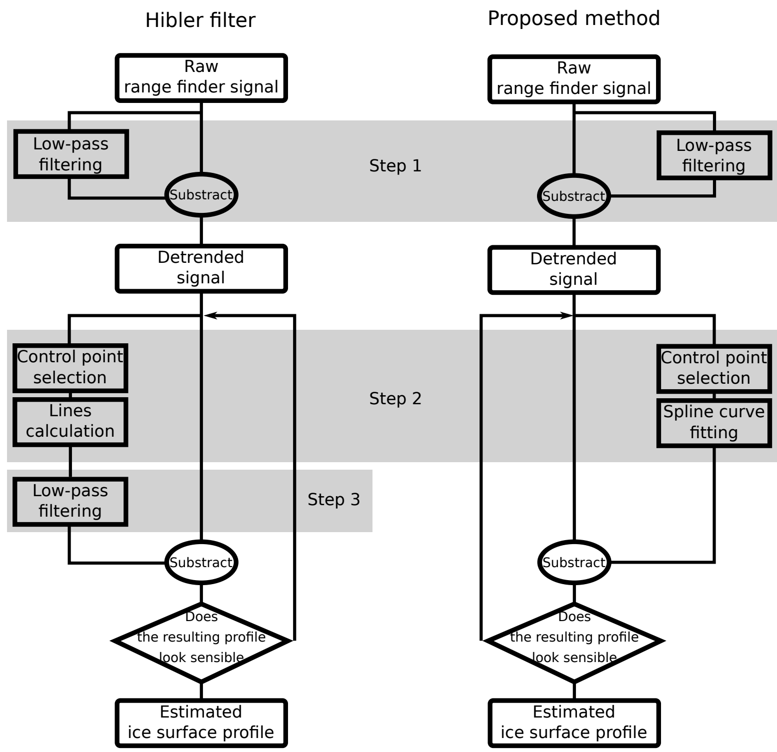

Figure 2: Filter process flowchart, from raw signal to the estimated ice surface profile. The left flowchart presents the Hibler filter while the right flowchart presents the proposed method.

the first approximation the vertical motion of a helicopter 2) curve fitting on reference point, similar in the initial approach to the Hibler filter (Fig.2). This proposed process significantly differs from the Hibler filter on the second step, directly estimating a curve instead of straight lines, and thus eliminate Hibler filter need for a low-pass filter at the third step to smooth the curve.

The first step actually consists of a low-pass filter to estimate a first estimation of the vertical profile of the helicopter motion and subtract it from the raw signal (Fig.2). This approach simplifies the adjustment of the filter cut-off wavelength by visual interpretation. At this step a zero phase Butterworth filter [14, 15] with a cut-off wavelength of 200 m is applied. A typical HEM flight is conducted with a speed of 30-40 m/sec; 200 m distance on the ground corresponds roughly to 5 seconds flying time, which could be considered a typical timescale for a short range aerodynamic turbulence to disturb the helicopter and the pilot reaction time to compensate for it. Depending on flight conditions and pattern, applicability of this cut-off wavelength should be assessed for each flight or even flight section, according to the main vertical pattern of the recorded signal. For example, less calm flying conditions may require a shorter cut-off wavelength to capture the more rapid changes in elevation of the aircraft. This first step ensures a proper selection of the reference points and allows for a better estimation of the helicopter motion component remaining in the signal, such as rapid altitude losses or altitude gains. The effect of the tuning of this cut-off wavelength will be further discussed in section 5.

On step 2, a spline function is fitted to a set of reference points to further generate a surface topography profile along the helicopter flight path. Reference points are automatically selected from the high-pass filtered raw LRF profile by identifying the local maxima on a sliding window of a fixed width. The number of selected reference points depends on this window length, so the window length has to be adjusted according to the recorded signal and the field notes (taken by the instrument operator during the flight) to guarantee the best results. Here, from visual interpretation of the flight profile and the plot of the selected points on the profile (Fig.3c), we selected a window of 175 m (corresponding to 500 measurement points), resulting in 66 reference points selected. We will discuss the tuning of the parameters in more detail

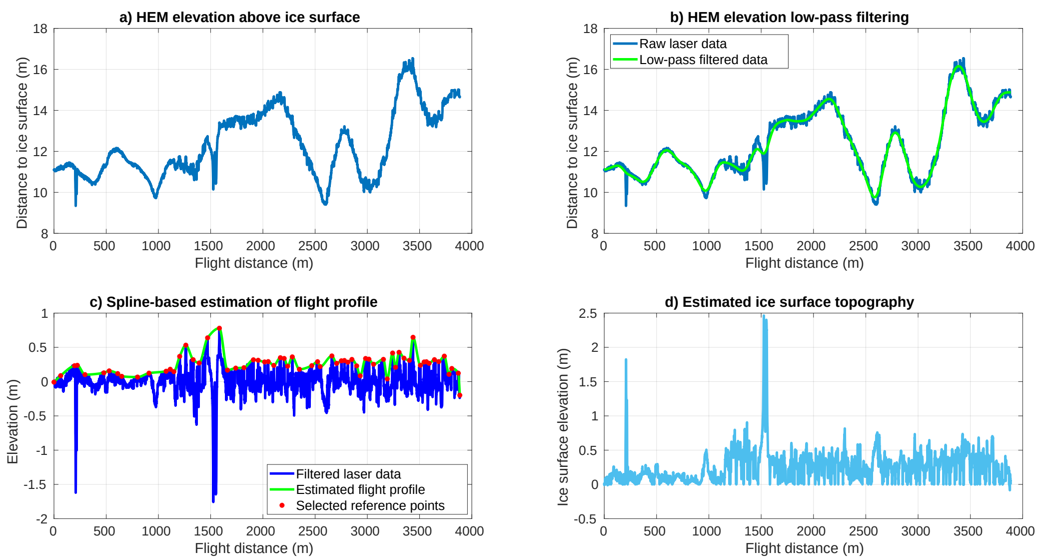

Figure 3: Example of the filtering workflow depicted in flowchart of Fig.2 applies on a 4 km flight section (see section 3 for details). The raw signal from LRF (blue line in a, b and c) is first detrended with a low-pass filter (green line in b) to help the selection of the reference points (red stars in c) for the calculation of the spline line (green line in c) representing the HEM vertical motion. The subtraction of the vertical motion leads to the estimation of the ice surface topography profile (purple line in d). The negative elevation at the end of the curve is the result of edge effects.

in the discussion section.

The superposition of the filtered signal generated in Step 1 and the spline curve is assumed to be representative of the vertical motion of the helicopter and can then be subtracted from the laser altimeter signal in order to reconstruct the sea ice surface topography.

3. Data

For testing the described method, we applied it to data from a section of an airborne survey in Fram Strait (Greenland Sea) over sea ice of the Norsk Øer Ice Barrier (Fig.4), a large fast ice area east of Greenland [16, 17]. The Fram Strait cruise is an annual interdisciplinary expedition led by the Norwegian Polar Institute along a transect at 78°50' N latitude between Svalbard and Greenland, consisting of research and monitoring within oceanographic, sea ice physics, biochemistry and selected biology studies [18, 19, 20]. Some years, it also comprises a helicopter for airborne survey. In 2016, the helicopter was equipped with both the HEM and the ICECam, a high resolution camera setup with a capability to reconstruct the along-the -track surface topography using photogrammetry. The combination of the two instruments allowed simultaneous acquisition of the sea ice thickness and surface topography. In this study, the ICECam data is used as a reference dataset to check the validity of the proposed filtering method.

3.1. Helicopter-borne electromagnetic ice thickness sensor (HEM)

The ice thickness sensor makes use of the principles of electromagnetic induction and the contrast of electrical conductivity of air and sea ice (low conductivity) on one hand and sea water (high conductivity) on the other

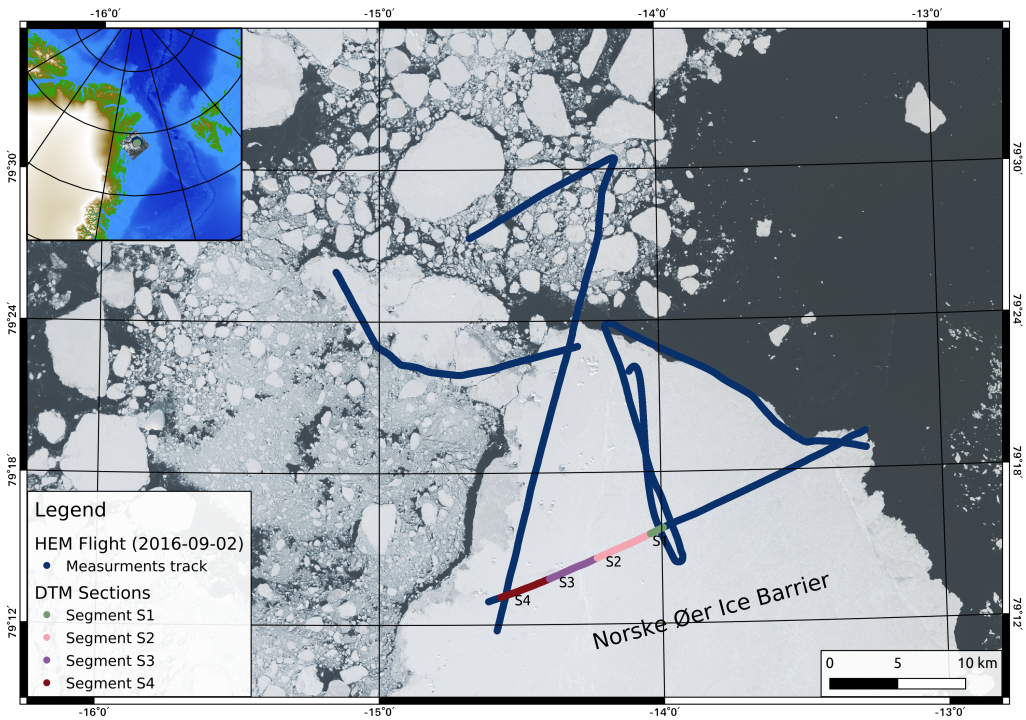

Figure 4: Map presenting the survey area, over sea ice of the Norske Øer Ice Barrier, east of Greenland. The marine blue represents the flight track with the HEM-measured total ice thickness (2 September 2016). Gaps in the track correspond to absence of measurements (either due to GPS signal loss or calibration of the instrument). The green, pink, purple and red sections represents the segments S1, S2, S3 and S4, respectively, where surface topography was reconstructed from ICEcam imagery using photogrammetric methods. The larger ice area marked "Norske Øer Ice Barrier" is static fast ice, an area of immobile sea ice anchored to several grounded icebergs, while the other ice in the image is mobile, drifting sea ice. Background: USGS/NASA Landsat 8 (7 September 2016)

hand [12]. Using a set of two coils (one transmitting and one receiving) allows deriving the distance from HEM to the bottom of the sea ice. The total ice thickness (ice plus snow) is calculated by subtracting the distance to the ice or snow surface to the distance inferred to the sea water. During the flight, the instrument is towed under the helicopter on a sling load of about 25 m (Fig.1), and has a typical altitude during measurements of around 15 m above the ice surface.

The distance to the ice surface is measured using a Riegl LD90-3100HS general purpose laser range finder mounted in the front of the instrument. This LRF emits a beam of infrared light (905 nm wavelength) [21] which is reflected by the top of the sea ice, or snow in the case of snow-covered sea ice. With current settings the LRF measures a distance to the ice surface with a sampling rate of 100 Hz and a typical accuracy of ± 3 cm [21, 22]. With a typical flying speed of 30 to 40 m/s, the horizontal sampling distance along the flight track varies from 30 to 40 cm.

Finally, position of the HEM during the flight is logged by an internal GPS receiver.

3.2. ICECam

3.2.1. Instrument

The main components of the ICECam system are two downward looking DSLR cameras, a GPS receiver, an inertial navigation system (INS) and a LRF. The system is fitted into an aerodynamic pod mounted in the front of the helicopter, with the GPS antenna mounted above the helicopter cockpit [23, 24].

The shooting framerate is set at 1 image per second for each camera.

At the typical flying altitude during HEM surveys, around 40 m over the ice surface for the helicopter, and the typical flying speed the camera parameters ensure a 50% to 70% overlap between the successive images with a footprint of approximately 60 m by 40 m, at an altitude of 40 m over the ice surface. This setup enables the reconstruction of the ice surface DTM, using photogrammetry techniques.

3.2.2. Processing ICECam data and generating the DTM

To increase the accuracy of the positioning of the photos for the generation of the DTM, the raw GPS and INS data is post-processed using the Precise Point Positioning (PPP) technique. This is achieved with the commercial software package TerraPos2 by TerraTec AS (Bergen, Norway). The resulting elevation is given relative to the ellipsoid [25, 26]. Since tidal and atmospheric effects can significantly affect the sea level, the ellipsoid-based positioning data is adjusted using corrected for pitch and roll LRF data. The typical offset between ellipsoid and ocean surface in the study area for the segments of the flight track with photogrammetrically reconstructed DTM is about 25 m. For simplicity, we will further call the the post-processed positioning data "GPS".

In order to build the DTM, the images are corrected for lens distortion and vignetting. More detail on the ICECam system, the processing and its accuracy can be found in [24]. Air refraction and Earth curvature are not taken into account due to the low altitude the surveys are carried out at. The reconstruction of the DTM is achieved using the commercial software package Socet GXP from BAE-Systems. On test campaigns, the DTM has proven to yield an RMS error of about 0.04 m and a bias of 0.03 m for the ice freeboard, the distance between ice surface and water level, in comparison to field measurements.

Since the processing and construction of the DTM is very time consuming and computer-intensive, only short sections have been processed. In this study, we are using four sections, called section S1 to S4 (Fig.4).

4. Results

In this section we show vertical motion and ice surface topography reconstruction results for the selected flight, and compare them with the data from the ICECam. The HEM and ICECam datasets represent independent observations, since no communication exists between the two instruments.

4.1. Helicopter vertical motion estimation

A flight altitude profile estimated using the proposed two-step approach can be assumed to be representative of the helicopter motion. However, the GPS profile from the ICECam is given relative to the ellipsoid and adjusted to the local surface with the average distance measured with the own ICECam LRF, while the estimated profile is relative to the water surface. To compare the two we will add the average difference between the two profiles to the estimated curve. Fig.5a presents the comparison between the ICECam GPS reference profile and the estimated profiles, for the four flight sections. Fig.5b-e present the scatter plots of the HEM estimated profile against the ICECam profile.

For all four segments, we notice that the two profiles do not overlap perfectly but the estimated profile looks reasonably similar the the GPS profile.

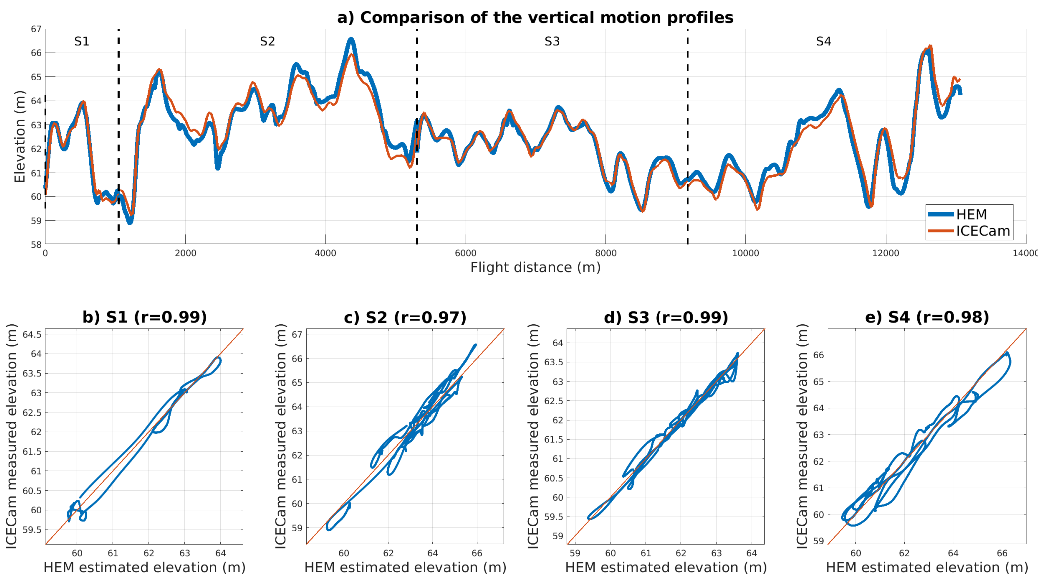

Figure 5: Comparison of the helicopter vertical motion estimation to the Precise Point Positioning flight altitude from the ICECam GPS+INS system. Plot a) represents the elevation data of the four segments (delimited by a vertical dashed line) for both the estimated motion (represented in blue) and the GPS profile (represented in red). The four plots b) c) d) and e) represent the scatter plots of the HEM estimated profile against the ICECam profile.

The correlation between the two profiles is systematically over 0.97 (Fig.5b-e). The high correlation confirms the first visual interpretation of Fig.5. We also calculated the mean absolute deviation and standard deviation of the difference between the two profiles for each section. With an average mean absolute deviation of 0.23 m (maximum of 0.33 m) and an average standard deviation of 0.27 m (maximum of 0.37 m) we are within the acceptable positioning uncertainty for a PPP solution for a vertical coordinate [27].

Since the vertical motion of the helicopter has been proven to be estimated within an acceptable precision, we can now in the next step use the HEM LRF to estimate the sea ice surface topography.

4.2. Sea ice surface topography reconstruction

The DTM generated from the photogrammetric reconstruction of ICE-Cam imagery is considered as the reference surface topography in this part for comparison with the profile estimated from the LRF. However, we acknowledge that a DTM calculated from photogrammetry may contain its own uncertainties and possible biases, and it does not represent an ideal ground truth.

To compare the surface profile estimated from the HEM LRF, the corresponding profile along the flight track was extracted from the DTM. Both datasets are represented by point measurements, but the DTM has a much higher spatial resolution than the HEM profile (5 cm for the DTM compared to 35 cm, on average, for the altimeter), so we choose to extract the matching profile by selecting the closest DTM point for each HEM point. The comparison between the two surface profiles is presented in Fig.6a.

Since the GPS vertical profile from the ICECam and the estimated helicopter motion are not identical, the differences are expected to propagate into the reconstructed ice surface. In the photogrammetrically reconstructed DTM profile, we noticed negative values for some lower elevations while one could expect the minimum values to match the sea level. It does not seem random but more associated to a low frequency variability. This is most likely the effect of uncertainties in the positioning and/or feature matching processing in the photogrammetric solution, such as a lack of local z-control points that causes biases in the vertical coordinate of the photogrammetric reconstruction, and lies within the accuracy of the PPP solution. However, to simplify the comparison with the HEM signal, we corrected this variability by subtracting the lower envelope to the signal, a spline curve passing by the lowest points in the signal, points assumed to correspond to the sea level. For the calculation of the spline curve we followed the same procedure as for the second step of our method.

Fig.6 demonstrates similarity between the ice surface topography estimated from the HEM signal and the corrected ICECam DTM, apart from a few exceptions in the DTM, probably corresponding to a crack in the ice or melt pond (e.g. Fig.6b at 1500 m). This feature does not appear in the HEM profile. The photos shows the edge of a meltpond, and few missing points in the raw laser data. Infrared LRF signals are known to drop over meltpond and open water. The reflected laser signal may then have been too weak for the instrument to register the return.

Few more local deviation can also be noted for the example at about 2600 m (Fig.6c). This is most-likely the result of a local envelope-filtering

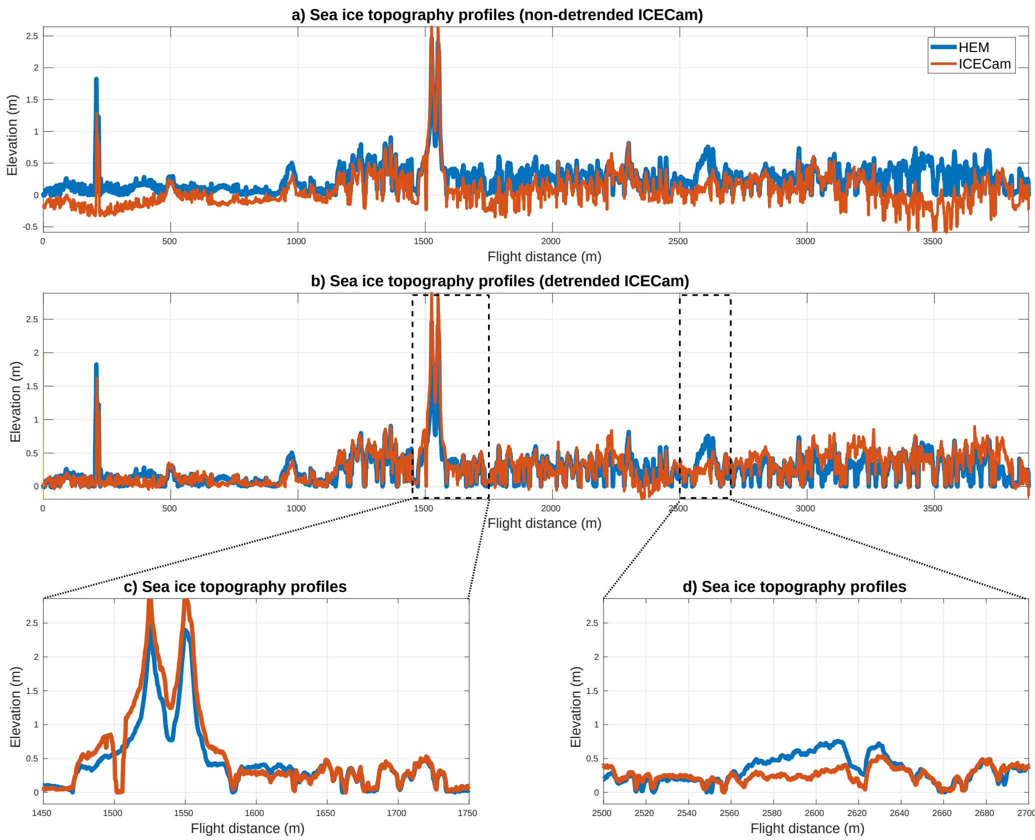

Figure 6: Comparison of the sea ice surface profiles, as estimated from the helicopter-borne electromagnetic sounder range finder (in blue) and the non-detrended ICECam (in red in plot a)) and detrended ICECam (in red in plot b)) for the flight segment S4. The rectangles in dashed-line in b) represents the bounding box of the zoomed version presented in c) and d).

artefact.

We applied the same procedure on all four flight segments (Fig.7). While segments S3 and S4 provide satisfactory results with a correlation between the two signals above 0.80, the two first segments seem less correlated, in particular the second segment. Since all the segments were batch-processed with the filtering parameters adjusted for the flight segment S4, a specific tuning for each segment could improve these results. However, the main features can still be recognised in all four segments. The standard deviation is 0.18 m on average (for a mean absolute bias is of 0.12 m on average), which is within acceptable margins (GPS PPP accuracy).

5. Discussion

5.1. Comparison with the Hibler filter

Since our proposed method is a modification of the Hibler filter, we compared the output of the two procedures, using the method presented here, and the Hibler filter. The first main difference is the number of parameters to adjust to achieve a satisfactory filtering. The Hibler filter is a three steps procedure, each steps having an adjustable parameter (Fig.2). By adding one parameter, the Hibler filter has more degrees of freedom and hence more ambiguous solutions. Moreover, being based on a succession of straight lines, the two first steps of the process generate a discontinued signal. The low pass filter of the third step is supposed to compensate for these discontinuities, but may introduce non-negligible distortions due to a generally smooth nature of the helicopter motion. The Hibler filter is then less adaptable to flights with strong altitudinal changes, as it can be expected with a helicopter. This

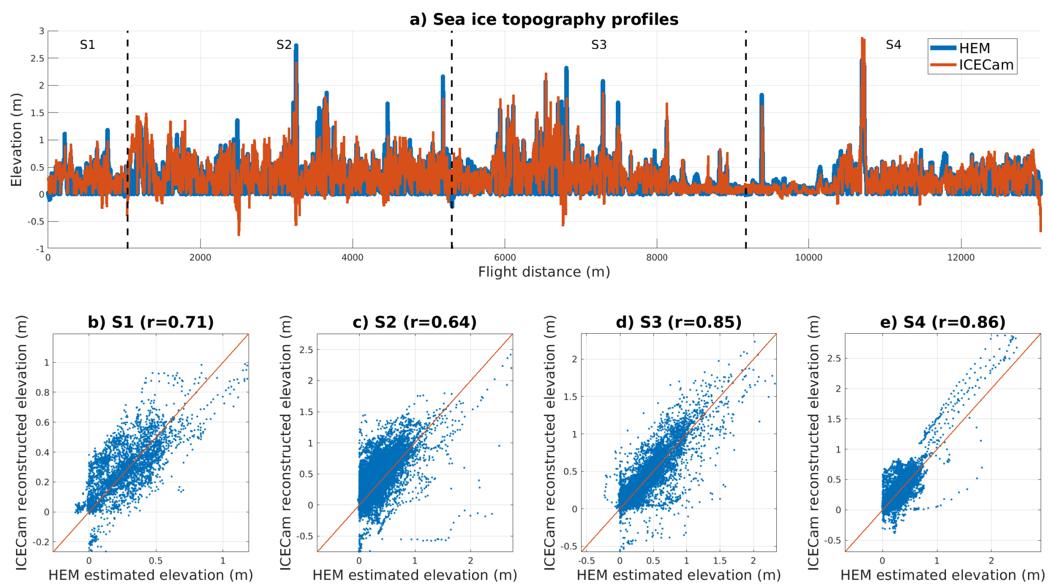

Figure 7: Comparison of the sea ice surface profiles, as estimated from the helicopter-borne electromagnetic sounder range finder using the Hibler filter (in blue) and the detrended ICECam (in red) for the four flight segments (a). The vertical lines delineate the different segments. The four plots b) c) d) and e) represent the scatter plots of the HEM estimated profile against the ICECam profile.

problem is however easier to solve when working on not too long flight sections, such as less than 1 km. The signal on such shorter sections presenting in general less variability, the parameters can be tuned more specifically for each flight segment.

For comparison with our filtering process, we applied the Hibler filter on the same sections of the flight. Fig.8a presents the estimated helicopter motion as well as the estimated ice surface for section S4 using the Hibler filter. As mentioned above, the filter has been difficult to tune properly. In particular, while choosing the right distance to select control points (Fig.2), we had to look for balance between strong distortions (with longer lines on step 2) and the underestimation of some topography (with shorter lines on step 2). The second option seemed to provide the most realistic ice topography.

The first 1000 m looks properly filtered, and the resulting ice surface profile presents very few negative values. However, when the altitude profile starts exhibiting mainly ridges with little to no level ice, the Hibler filter performance drops significantly. This can also be seen on the estimated ice surface on Fig.8b. After the first 1000 m, the number of negative values increases significantly. The correlation (0.73) appears weaker than with our filter and both the bias (± 0.16 m) and standard deviation (0.19 m) are also higher than with our filter. We can note these results do not discard the applicability of the Hibler filter but confirm our method provides improvements in the quality of the final product.

As previously, we repeated the comparison process over the four segments of flights (Fig.9). The results appear similar for the four flight segments. The average correlation (0.66) is lower than with our filter and both the bias

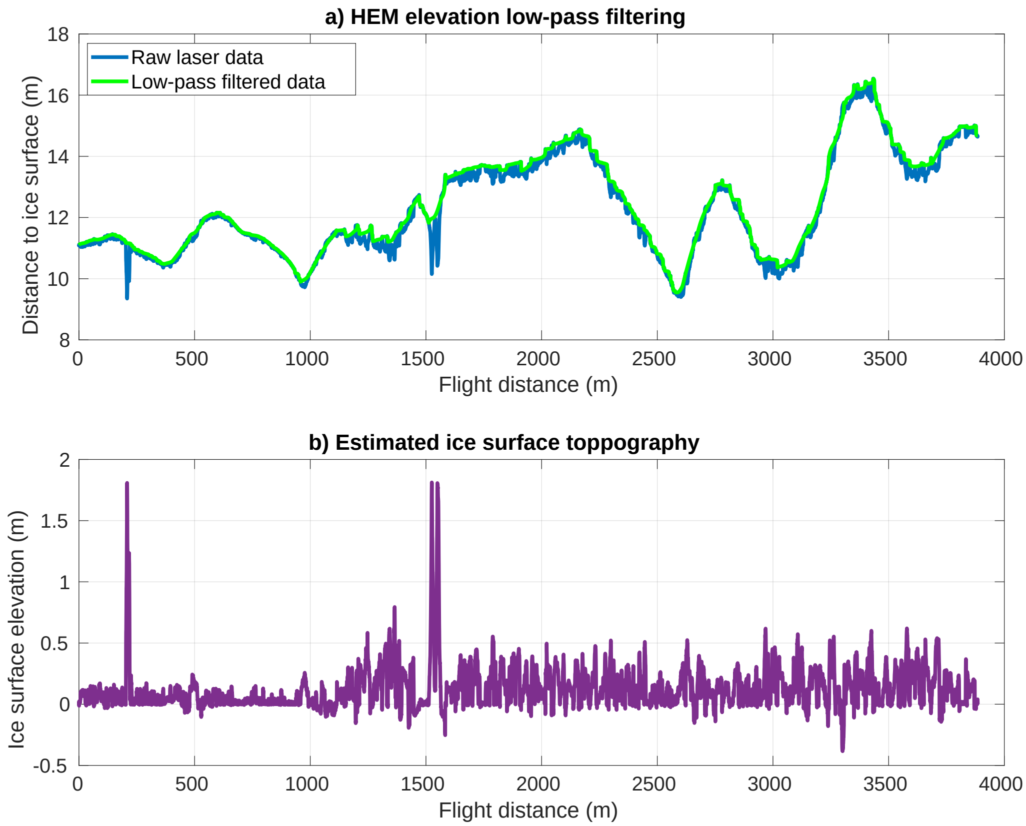

Figure 8: Filtering of the section S4 using the Hibler filter. a) Raw signal from the LRF and the helicopter motion estimated using the Hibler filter. b) Estimated ice surface topography.

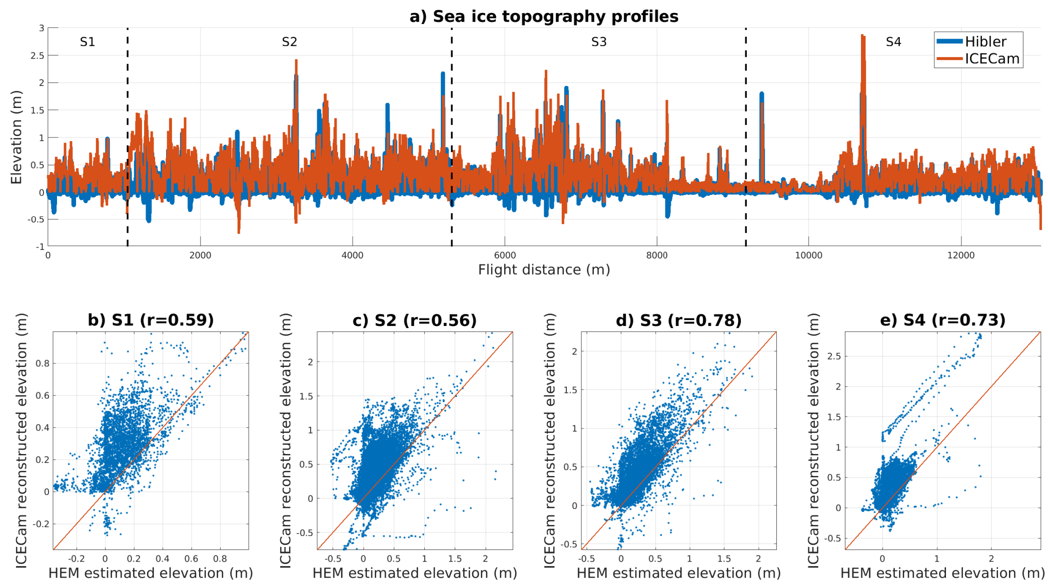

Figure 9: Comparison of the sea ice surface profiles, as estimated from the HEM LRF using the Hibler filter (blue) and the detrended ICECam (red) for the four flight segments. The vertical lines delineates the different segments.

($\pm 0.19\,\mathrm{m}$) and the standard deviation ($0.20\,\mathrm{m}$) are higher.

We calculated the distribution of the estimated ice surface elevation for the ICECam data and the two filtering method, for each segments of flights (Fig.10). Our filtering method appears to generally match the ICECam distribution for the segments S3 and S4. Our method seems to over-estimate the amount of zero-elevation data on both segments S1 and S2. It also misses a second mode around $0.25\,\mathrm{m}$ on segment S1 while presenting one not present in the ICECam data on S2. The Hilber method consistently over-represents the lower elevation while under-estimating everything above $0.25\,\mathrm{m}$. This is consistent with the choice we had to make when adjusting the filter parameters, in particular the line length in the second step.

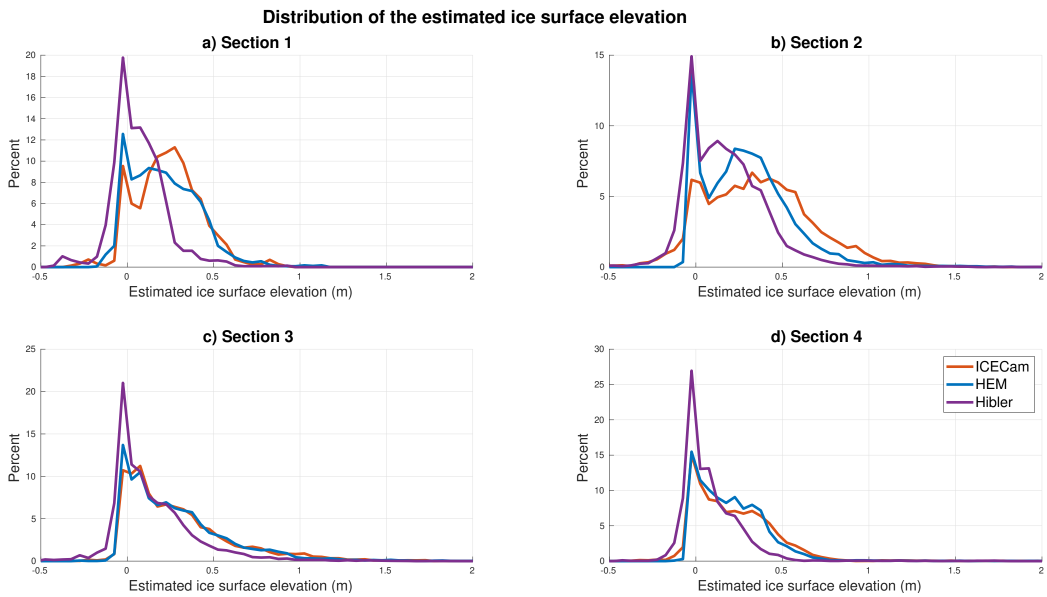

Figure 10: Comparison of the sea ice surface elevation distribution, as estimated from the detrended ICECam (red), our filtering method (blue) and the Hibler filter (purple) and for the four flight segments.

	ICECam		Proposed filter				Hibler			
			Elevation		Bias		Elevation		Bias	
	mean	std	mean	std	mean	std	mean	std	mean	std
S2	0.29	0.19	0.26	0.20	0.21	0.27	0.12	0.16	0.24	0.24
S2	0.41	0.32	0.34	0.27	0.32	0.42	0.22	0.23	0.35	0.41
S3	0.34	0.31	0.33	0.30	0.25	0.37	0.19	0.24	0.26	0.36
S4	0.27	0.28	0.26	0.23	0.19	0.28	0.13	0.18	0.21	0.29

Table 1: Comparison of the ice surface elevation statistics as estimated by the ICECam and the HEM LRF using both our proposed filtering method and Hibler filter.

Overall, the ice surface elevation statistics for all four flight segments, as well as bias, appears in favour of our method (Tab.1).

5.2. Adjusting the filtering parameters

The main challenge we experienced in this procedure is to manage to adjust the Hibler's filter parameter to reach acceptable results. As mentioned previously, the extra degree of freedom leads to a higher sensitivity of the method at the expense of labor intensity. Therefore we had to spend a large amount of time to adjust the parameters for the results presented here. However, the method proposed in this study also shows to be sensitive to the filtering parameters.

In our method, the first step (low-pass filter, Fig.2) of the filter plays an important role. If the main component of the helicopter movement is not filtered, the amplitudes of the variations are too strong. The spline curve then tends to oscillate and results is strong distortion of the final signal. But the overall process remains less sensitive to the cut-off frequency at this step.

Our empirical estimation of this parameter allowed us to remove most of the helicopter motion and no readjustment was required.

The sliding window length to select the control points is the most crucial parameter. If we select too many points (with a shorter sliding window), the spline curve will tend to follow small variations in the laser signal and underestimate the height of pronounced topographic features such as ice ridges. On the other hand, selecting a window too large will result in too few control points and prevent the curve to match properly the laser signal. This can lead to distortions and negative values of the ice surface elevation. Optimal choices for these processing variables depends to a high degree on the nature of the sea ice in a region, including the ice concentration, and the flight conditions and quality of the raw data.

The results from the processing of the airborne data are further on compared to field notes and on-flight imagery if available, in particular to check if the ridges and the leads are correctly represented in the final ice surface topography. If the results do not match the field notes, the length of the sliding window may be adjusted accordingly to reach the expected results. The adjustment of the first cut-off frequency should only be considered if the intermediate signal still presents significant low-frequency amplitudes.

To analyse the impact of the filtering parameters, we applied the proposed method on each of the four flight segments using a filter cut-off wavelength (Step 1, Fig.2) and sliding window length for the control points selection (Step 2, Fig.2) ranging from 10 m to 1500 m (with a 10 m step). Each resulting estimated ice surface is compared to the ICECam DTM. The corresponding absolute bias and standard deviation are calculated and plotted in a matrix (Fig.11). Contour lines are added on each plot panel to delineate 0.15 m and 0.25 m thresholds. For each of the four flight segments, the lower values of absolute bias are mainly found in a band corresponding to a filter cut-off wavelength ranging from 100 m to 400 m. However, the sliding window length seems to play only little role on the bias. This can be explained by the magnitude of variation each step of the filter is working. The first step aims to remove a signal having an amplitude of several meters, while the second step filters amplitude of less than a meter. In particular, we can notice that our 200 m cut-off wavelength for the first step appears suitable for all the flight segments while the window length should be adjusted for each segments. The window length parameter seems to play a more important role in the standard deviation. Here again, a common 200 m cut-off wavelength for the first filtering step provide good results for all the flight segments while the window length need to be adjusted for each segments to reach the best possible result (ranging from almost 700 m for S1 to 200 m for S2).

5.3. Laser range finder over open water

The HEM LRF emit pulses at infrared wavelength. This wavelength is poorly reflected by sea water, then the returned signal to the instrument can be too weak to be registered. In such case the instrument records a "missing value". It can result in fewer valid values recorded over leads and melponds, when they are melted through. This can pose an issue for the filtering procedure since it is based upon the assumption the lower values in the laser signal represent the sea water level. In practice, the LRF often manage to record few points, and the field notes can help identifying the leads

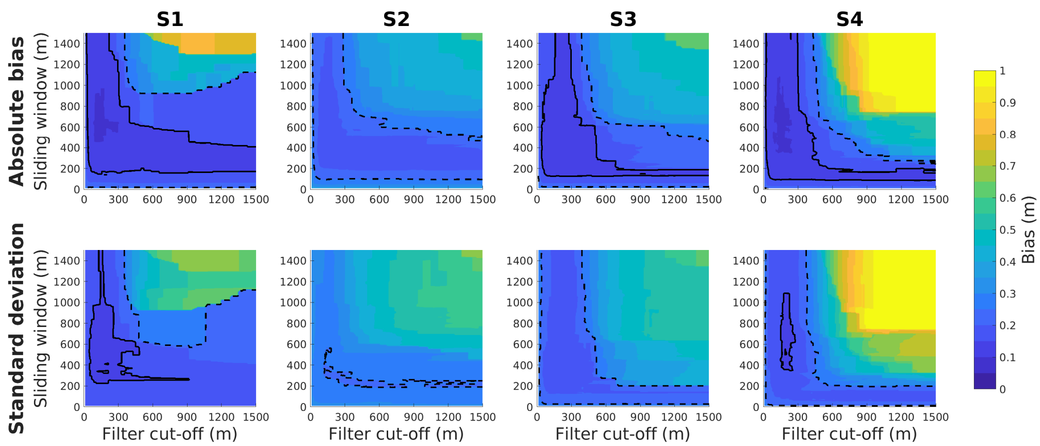

Figure 11: Absolute bias and standard deviation of the estimated ice surface topography transects, compared to the ICECam DTM, for filtering parameters ranging from 10 m to 1500 m for the four flight segments S1-4. The solid black contour line represents a 0.15 m threshold and the dashed black contour line a 0.25 m threshold.

and check which portion of the signal is missing. When only short distances are missing, an interpolation can then be used to compensate for the missing data. Longer missing segments are unlikely to happen since helicopter pilots usually avoid flying at low measurement altitude over open water.

In the eventuality of such long missing segments, in the order of a hundred meters or more, interpolation seems unreasonable and the signal should then be treated as two different flight segments.

5.4. Transects without open water

Since recording over open water is important to estimate the reference level for the helicopter motion, a flight happening over packed ice and vast sea ice floes without any openings also poses a problem. In such case, we have to assume the level ice to be parallel to the water surface and use it as a reference. Although the relative changes in the topography of the ice surface is preserved, which would be sufficient for applications such as, for example, snow drift or radar back-scattering models, the overall heights above sea level will be underestimated. In practice, open water and leads are usually found around the ship from where helicopter-borne surveys start. By actively choosing such area in a transect, a reference level can be recorded ensuring better result from the method.

6. Conclusion

We investigated a spline-based helicopter motion filter to estimate the sea ice surface topography from laser range finder. The filter is inspired of the widely used three-steps Hibler filter [13]. Our proposed method shares its first step with the Hibler filter, but differs at the second steps by using a spline line instead of a succession of straight segments. This eliminates the problem of discontinuities in the signal and the need for a third step to smooth the discontinuities with a low-pass filter, and thus an extra tuning parameter.

We tested our method on data collected during an NPI expedition to Fram Strait in 2016 and compared it to a DTM generated from stereo-photogrammetry data collected simultaneously and independently from the HEM data. The stereo-photogrammetry system incorporates a GPS which also gives us a reference for the helicopter vertical motion. In both cases, helicopter vertical motion and ice surface topography, the mean absolute bias of our model falls under the expected accuracy of GPS Precise Point Positioning reprocessing.

Although the Hibler filter gave overall satisfactory results, our procedure systematically resulted in a lower absolute bias. Furthermore, we experienced the spline-based filter easier to tune, having less parameters to adjust (two instead of three). This is an advantage when processing longer flight segments (several kilometers) and helicopter-borne surveys, helicopter being able to change altitude more abruptly than planes.

The method could only be tested on four flight segments, for a total distance of 13 km, presenting overall similar ice conditions. As a next step, a comparison using more diverse ice conditions could help to better identify the limitation of such procedure, in particular in different sea ice conditions, with a variety of ice concentration and sea ice types and features.

Appendix A. Acknowledgements

The authors are grateful to the crew and science team on board R/V Lance, in particular Marius Bratrein (NPI) and Anja Rösel (NPI, now DLR) who conducted the HEM surveys, as well as the helicopter pilots from Airlift AS. This research is funded by the Research Council of Norway (Center for Integrated Remote Sensing and Forecasting for Arctic operations, CIRFA SFI grant no. 237906) and CIRFA partners, and the Fram Centre project ALSIM (Automised Large-scale Sea Ice Mapping) in the Fram Centre "Sea ice in the Arctic Ocean, Technology and Governance" flagship.

The Matlab script of the filter function is available on Github: `https://github.com/jnegrel/HeliFilter`. The data used for this study is available upon request.

References

[1] T. Vihma, Effects of Arctic sea ice decline on weather and climate: A review, Surveys in Geophysics 35 (5) (2014) 1175–1214. doi:https://doi.org/10.1007/s10712-014-9284-0.

[2] W. N. Meier, G. K. Hovelsrud, B. E. van Oort, J. R. Key, K. M. Kovacs, C. Michel, C. Haas, M. A. Granskog, S. Gerland, D. K. Perovich, A. Makshtas, J. D. Reist, Arctic sea ice in transformation: A review of recent observed changes and impacts on biology and human activity, Reviews of Geophysics 52 (3) (2014) 185–217. arXiv:https://agupubs.onlinelibrary.wiley.com/doi/pdf/10.1002/2013RG000431, doi:https://doi.org/10.1002/2013RG000431.

URL https://agupubs.onlinelibrary.wiley.com/doi/abs/10.1002/2013RG000431

[3] G. Castellani, C. Lüpkes, S. Hendricks, R. Gerdes, Variability of Arctic sea-ice topography and its impact on the atmospheric surface drag, Journal of Geophysical Research: Oceans 119 (10) (2014) 6743–6762. doi:https://doi.org/10.1002/2013JC009712.

[4] I. A. Renfrew, C. Barrell, A. D. Elvidge, J. K. Brooke, C. Duscha, J. C. King, J. Kristiansen, T. L. Cope, G. W. K. Moore, R. S. Pickart, J. Reuder, I. Sandu, D. Sergeev, A. Terpstra, K. Våge, A. Weiss, An evaluation of surface meteorology and fluxes over the Iceland and Greenland Seas in ERA5 reanalysis: The impact of sea ice distribution, Quarterly Journal of the Royal Meteorological Society 147 (734) (2021) 691–712. doi:https://doi.org/10.1002/qj.3941.

[5] P. Rampal, J. Weiss, D. Marsan, Positive trend in the mean speed and deformation rate of Arctic sea ice, 1979–2007, Journal of Geophysical Research: Oceans 114 (C5) (2009). doi:https://doi.org/10.1029/2008JC005066.

[6] G. E. Liston, C. Polashenski, A. Rösel, P. Itkin, J. King, I. Merkouriadi, J. Haapala, A distributed snow-evolution model for sea-ice applications (snowmodel), Journal of Geophysical Research: Oceans 123 (5) (2018) 3786–3810. doi:https://doi.org/10.1002/2017JC013706.

[7] J. Landy, J. Ehn, M. Shields, D. Barber, Surface and melt pond evolution on landfast first-year sea ice in the Canadian Arctic archipelago,

Journal of Geophysical Research: Oceans 119 (5) (2014) 3054–3075. doi:https://doi.org/10.1002/2013JC009617.

[8] A. Scagliarini, E. Calzavarini, D. Mansutti, F. Toschi, Modelling sea ice and melt ponds evolution: sensitivity to microscale heat transfer mechanisms, in: Mathematical Approach to Climate Change and its Impacts, Springer, 2020, pp. 179–198.

[9] S. M. Hvidegaard, R. Forsberg, Sea-ice thickness from airborne laser altimetry over the Arctic Ocean north of Greenland, Geophysical Research Letters 29 (20) (2002) 13–1–13–4. doi:https://doi.org/10.1029/2001GL014474.

[10] K. A. Giles, S. M. Hvidegaard, Comparison of space borne radar altimetry and airborne laser altimetry over sea ice in the Fram Strait, International Journal of Remote Sensing 27 (15) (2006) 3105–3113. doi:https://doi.org/10.1080/01431160600563273.

[11] J. F. Beckers, A. H. Renner, G. Spreen, S. Gerland, C. Haas, Sea-ice surface roughness estimates from airborne laser scanner and laser altimeter observations in Fram Strait and north of Svalbard, Annals of Glaciology 56 (69) (2015) 235—-244. doi:https://doi.org/10.3189/2015AoG69A717.

[12] C. Haas, J. Lobach, S. Hendricks, L. Rabenstein, A. Pfaffling, Helicopter-borne measurements of sea ice thickness, using a small and lightweight, digital EM system, Journal of Applied Geophysics 67 (3) (2009) 234–241.

[13] W. D. Hibler III, Removal of aircraft altitude variation from laser profiles of the Arctic ice pack, Journal of Geophysical Research (1896-1977) 77 (36) (1972) 7190–7195. doi:https://doi.org/10.1029/JC077i036p07190.

[14] A. M. Johansson, J. A. King, A. P. Doulgeris, S. Gerland, S. Singha, G. Spreen, T. Busche, Combined observations of Arctic sea ice with near-coincident colocated X-band, C-band, and L-band SAR satellite remote sensing and helicopter-borne measurements, Journal of Geophysical Research: Oceans 122 (1) (2017) 669–691.

[15] T. Yitayew, W. Dierking, D. Divine, T. Eltoft, L. Ferro-Famil, A. Rösel, J. Negrel, Validation of sea-ice topographic heights derived from TanDEM-X interferometric SAR data with results from laser profiler and photogrammetry, IEEE Transactions on Geoscience and Remote Sensing 56 (11) (2018) 6504–6520. doi:http://doi.org/10.1109/TGRS.2018.2839590.

[16] W. A. Sneed, G. S. Hamilton, Recent changes in the norske Øer ice barrier, coastal northeast Greenland, Annals of Glaciology 57 (73) (2016) 47–55. doi:https://doi.org/10.1017/aog.2016.21.

[17] C. Wang, J. Negrel, S. Gerland, D. Divine, P. Dodd, M. A. Granskog, Thermodynamics of fast ice off the northeast coast of Greenland (79°N) over a full year (2012–2013), Journal of Geophysical Research: Oceans 125 (7) (2020) e2019JC015823. doi:https://doi.org/10.1029/2019JC015823.

[18] A. H. H. Renner, S. Gerland, C. Haas, G. Spreen, J. F. Beckers, E. Hansen, M. Nicolaus, H. Goodwin, Evidence of arctic sea ice thinning from direct observations, Geophysical Research Letters 41 (14) (2014) 5029–5036. doi:https://doi.org/10.1002/2014GL060369.

[19] L. de Steur, C. Peralta-Ferriz, O. Pavlova, Freshwater export in the east greenland current freshens the north atlantic, Geophysical Research Letters 45 (24) (2018) 13,359–13,366. doi:https://doi.org/10.1029/2018GL080207.

[20] G. Spreen, L. de Steur, D. Divine, S. Gerland, E. Hansen, R. Kwok, Arctic sea ice volume export through fram strait from 1992 to 2014, Journal of Geophysical Research: Oceans 125 (6) (2020) e2019JC016039. doi:https://doi.org/10.1029/2019JC016039.

[21] C. Von Saldern, C. Haas, W. Dierking, Parameterization of Arctic sea-ice surface roughness for application in ice type classification, Annals of Glaciology 44 (2006) 224–230. doi:https://doi.org/10.3189/172756406781811411.

[22] Riegl, Ld90-3100hs datasheet, `http://www.riegl.com/uploads/tx_pxpriegldownloads/LD90-3_alldatasheets_for_website_25-03-2010.pdf` (2010).

[23] D. V. Divine, M. A. Granskog, S. R. Hudson, C. A. Pedersen, T. I. Karlsen, S. A. Divina, A. H. H. Renner, S. Gerland, Regional melt-pond fraction and albedo of thin Arctic first-year drift ice in late summer, The

Cryosphere 9 (1) (2015) 255–268. doi:https://doi.org/10.5194/tc-9-255-2015.

[24] D. V. Divine, C. A. Pedersen, T. I. Karlsen, H. F. Aas, M. A. Granskog, S. R. Hudson, S. Gerland, Photogrammetric retrieval and analysis of small scale sea ice topography during summer melt, Cold Regions Science and Technology 129 (2016) 77 – 84. doi:https://doi.org/10.1016/j.coldregions.2016.06.006.

[25] National Geodetic Survey (NGS), Geodetic glossary, `https://www.ngs.noaa.gov/CORS-Proxy/Glossary/xml/NGS_Glossary.xml`, (Updated: May 15, 2019) (2001).

[26] G. Wang, T. Soler, Measuring land subsidence using GPS: Ellipsoid height versus orthometric height, Journal of Surveying Engineering 141 (2) (2015) 05014004. doi:https://doi.org/10.1061/(ASCE)SU.1943-5428.0000137.

[27] M. G. Wing, J. Frank, Vertical measurement accuracy and reliability of mapping-grade GPS receivers, Computers and Electronics in Agriculture 78 (2) (2011) 188 – 194. doi:https://doi.org/10.1016/j.compag.2011.07.006.